High Resolution Profiling Using Ion Scattering and Resonant Nuclear Reactions.

R.P. Pezzi

Instituto de Física - Universidade Federal do Rio Grande do Sul - Brazil

R.M. Wallace

Department of Electrical Engineering and Physics, University of Texas at Dallas

M. Copel

IBM Research Division, T. J. Watson Research Center, Yorktown Heights, NY

I.J.R. Baumvol

Universidade de Caxias do Sul, CCET and Universidade Federal do Rio Grande do Sul – Brazil

Abstract. This paper presents the basic principles of medium energy ion scattering and of nuclear resonant reaction profiling, which at present constitute available techniques for near-surface elementary profiling with high depth resolution. The principles of ion energy loss are discussed at first, as they constitute the basic physical processes underlying the profiling techniques. Examples are presented and discussed, mainly concerning applications in the area of high-k replacement materials for silicon oxide/oxinitride in ULSI technology. The possibility of profiling elements with nano or subnanometric resolution is giving a significant contribution to solve many problems of research and development in MOS structures for advanced ULSI technology.

Keywords: Depth profiling; Medium energy ion scattering; Resonant Nuclear Reaction Analysis.
PACS: 34.10+x, 34.50.Bw

INTRODUCTION

Quantitative determination of depth distribution of different chemical species with nano or subnanometric resolution has become an important tool for ULSI research and development. This is especially useful in structures that hold uniform lateral distribution. Among the species of interest one can mention: i) light - N, O, Si, and Al - and heavy - Zr, Hf, La, and other - elements that form the new metal oxides, silicates, nitrided silicates, and aluminates compound materials considered for gate dielectric replacements to silicon oxide/oxinitride, ii) B, Al, P, Si, Ti, Mo, As, Sb and other species, used as dopants of ultrashallow source and drain Si regions, as well as of new metallic, intemetallic, and compound gate electrodes.

In recent years, triggered by the demand from ULSI technology, nondestructive methods based on ion beams at intermediate energies have been dedicated to this task. The most well known technique is medium energy ion scattering (MEIS). In addition, when light species are involved, narrow nuclear resonant reaction profiling (NRP) is also used. The aim of the present article is to discuss the

CP 788, *Characterization and Metrology for ULSI Technology 2005,*
edited by D. G. Seiler, A. C. Diebold, R. McDonald, C. R. Ayre, R. P. Khosla, S. Zollner, and E. M. Secula

fundamentals of these methods, together with some examples that show their potentialities and synergisms.

ION ENERGY LOSS

Methods for profiling based on ion beams at intermediate energies rely on the fact that energetic ions penetrating solid matter progressively loose energy, the energy loss being rather well known and capable of being predicted. Figure 1 shows a sketch of the physical situation. More specifically, when an energetic ion reaches a solid material, several scattering events take place. These events result from two major binary interactions, namely ion-atom and ion-electron interactions, which bring about ion kinetic energy loss and deflection from the original path. There are two principal observables of the energy loss process: i) the average ion energy transferred per unit of trajectory length, the stopping power, dE/dx, and ii) the broadening of the ion energy distribution as it penetrates deeper in the solid, referred to as the straggling constant, S^2. The values of dE/dx and S^2 for a given target depend on the ion state (kinetic energy, mass, atomic number, charge state) and on target composition. Fig. 1 shows also the energy dependence of the two main energy loss processes. The reason for using ion beams at intermediate energies can be clearly seen by inspection of Fig. 1: it is the ion energy range where dE/dx for most combinations of ion and solid materials reach their maxima, which on its turn will lead to maximum depth resolution.

Ion-atom interactions are modeled as classical elastic collisions between two point particles, resulting in energy transfer and deflection. On the other hand, a more refined probabilistic approach is required in the modeling of ion-electron interactions. The usual approach supposes that the number of ion-electron interactions is sufficiently large to allow one to use the central limit theorem. Thus, details of energy transfer during each individual ion-electron interaction are not relevant and a Gaussian ion energy distribution law may be used. However, when the main interest is on thinner, near surface regions of the solids the number of ion-electron binary encounters decreases and consequently the Gaussian approximation fails to predict the energy loss laws. Details of individual ion-electron interactions must then be taken into account, and the energy loss laws can be obtained by modeling the physical processes using stochastic theory of electronic energy loss.

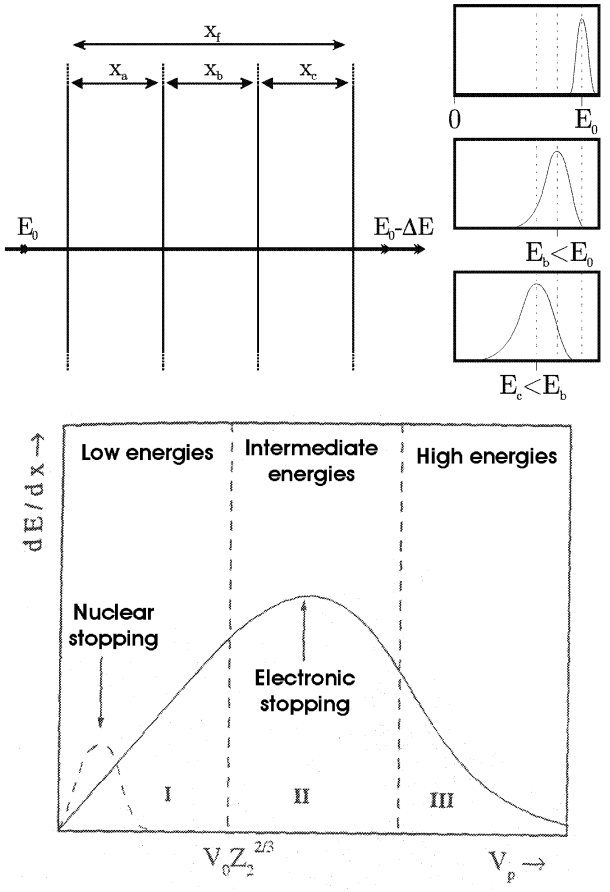

FIGURE 1. (top) a sketch of the physical picture of ion energy loss in solids and (bottom) energy dependence of the two main energy loss processes.

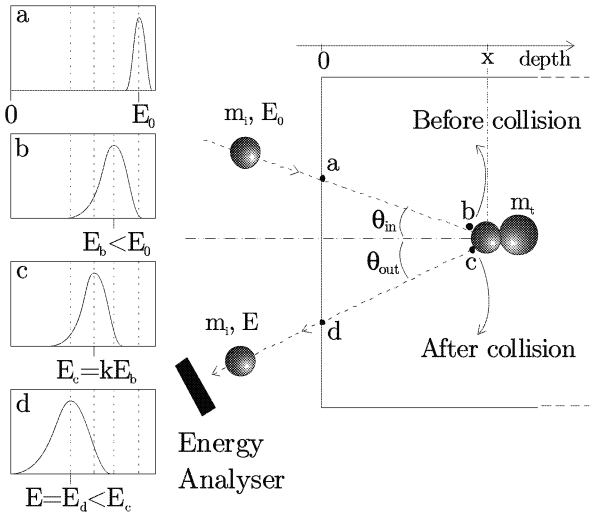

FIGURE 2. A typical MEIS arrangement. Sketches of energy loss laws at selected points are shown in the insets.

MEDIUM ENERGY ION SCATTERING

Ion-atom interactions can lead to very large angle deflections in one single collision that eventually directs the ion backward, toward the sample surface as depicted in Fig. 2, where a typical medium energy ion scattering (MEIS) arrangement is shown. The kinetic energy spectrum of the emerging ions is usually determined with high resolution by electrostatic energy analyzers. An adequate expression of the ion energy loss law contains, among many other variables including instrumental ones, the depth distribution of the scatterer species. The number $N_i(E)$ of scattered ions emerging with energy E from the sample surface, after a head on collision with a nuclide of species i is calculated within a stochastic modeling framework to give:

$$N_i(E) = n_0 \Omega \xi \sigma_i \int_0^{\infty} C_i(x) \sum_{n,l} K_n^{in} K_l^{out} f_{in}^{*n} * f_{out}^{*l}$$

where n_0 is the number of incident ions, Ω and ξ are the detection solid angle and efficiency, respectively, σ_i is the scattering cross-section, $C_i(x)$ the concentration distribution in depth of atomic species i, f^{*n} is the nth auto-convolution of the normalized collision spectrum (calculated with the Rutherford electron scattering theory) with itself, and K_n^{in} and K_l^{out} are the weights of the n_{th} ingoing and l_{th} outgoing convolutions,

$$K_n = \frac{(mx)^n}{n!} e^{-mx}$$

The results are exemplified in Fig. 3, which shows the calculated energy spectra of 100 KeV protons scattered from Hf atoms present in hypothetical Hf delta layers immersed in a pure Si matrix at different depth, namely 0.5, 1.5, 3, and 5 nm (top), as well as on a 0.8 nm SiO_2 film on Si (bottom). One can estimate the depth resolution for this kind of measurement, obtained in a MEIS experimental arrangement with a good electrostatic energy analyzer, as approximately 0.5 nm near the surface. Straggling of the ion beam energy causes degradation of the depth resolution in deeper regions below the surface. Gaussian approximation calculations are shown in each case. In Fig. 4, stochastic and Gaussian approximation calculations are used to simulate experimental scattering spectra of 100 KeV protons incident on homogeneous, flat 1, 2, 4, and 8 monolayers of Bi deposited on Si.

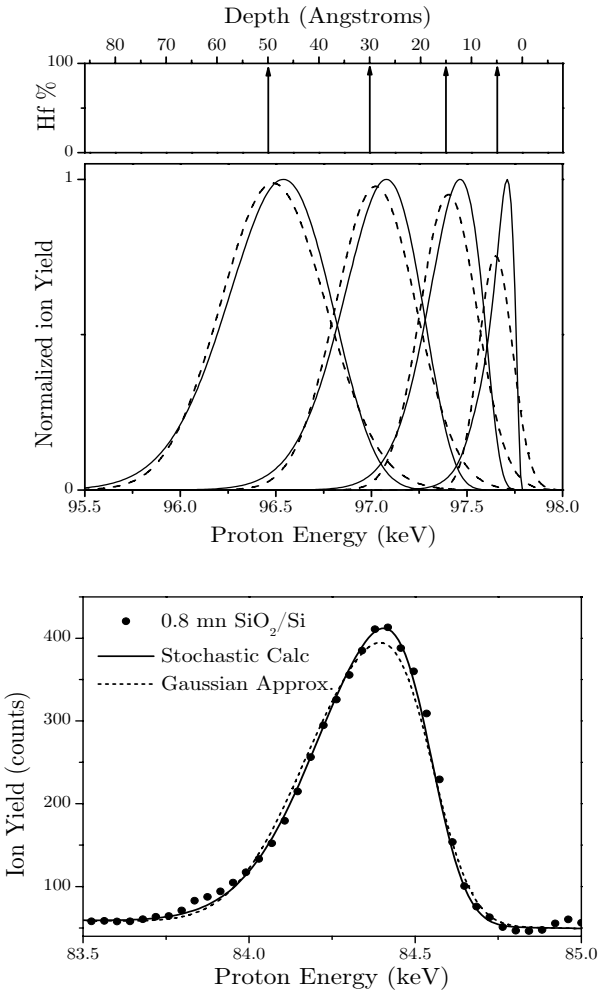

FIGURE 3. Calculated energy spectra of 100 KeV protons scattered from (top) Hf atoms present in hypothetical Hf delta layers immersed in a pure Si matrix at different depths and (bottom) from a 0.8 nm SiO_2 film on Si with the corresponding experimental data (solid dots). The solid and dashed lines stand for the stochastic and Gaussian calculations, respectively.

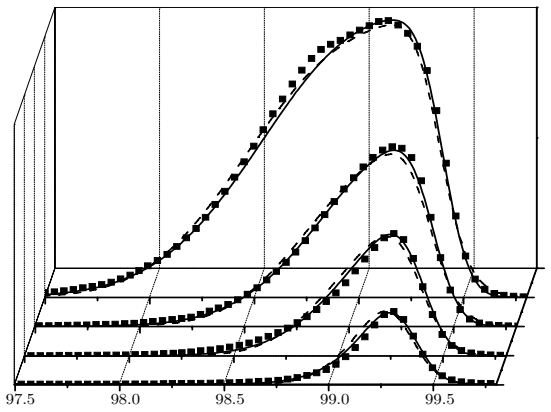

FIGURE 4. Experimental points (solid dots), stochastic (solid lines) and Gaussian (dashed lines) simulations of 100 KeV protons incident scattered from homogeneous, flat 1, 2, 4, and 8 monolayers of Bi deposited on Si (111).

MEIS is being largely used in the research of high-k materials for gate dielectric. There are many examples and Fig. 5 illustrates such application. It shows MEIS spectra of as-deposited and air annealed $(La_2O_3)(SiO_2)$ films deposited on Si by reactive co-evaporation. From the spectra it is apparent that there is no dissociation of the compound film after annealing at 850°C. The difference between as-deposited and annealed spectra is the increased width of the signals corresponding to oxygen and silicon; this increase occurs at the low energy side of the O and Si peaks, below the original silicate layer, indicating subsurface silica formation. In addition, the La spectrum itself is now broader (distributed deeper in the film). This last could occur because of roughness in the overlayer or because some of the interfacial La has diffused down, making a more Si-rich lanthana silica alloy.

We recall that in all experimental MEIS results shown above the incident proton beam and detection axes were aligned with one of the crystalline directions of the underlying Si single crystalline substrate, which substantially lowers substrate contribution to the scattering spectra.

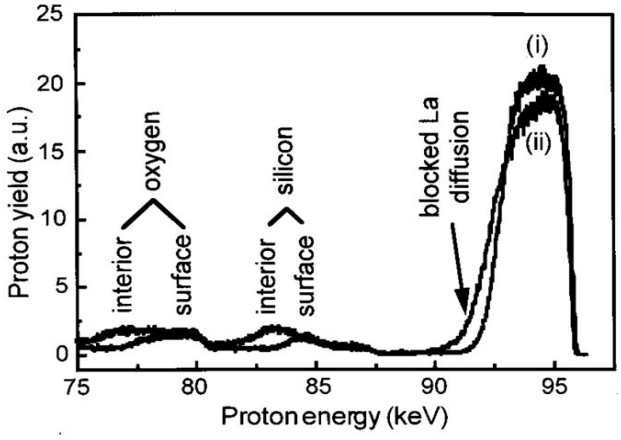

FIGURE 5. MEIS spectra for $(La_2O_3)(SiO_2)$ film deposited on Si by reactive co-evaporation (i) and then annealed in air (ii).

NARROW NUCLEAR RESONANT REACTION PROFILING

The same phenomena of electronic ion energy loss, described by the same laws that are obtained from a detailed stochastic modeling, can be used in an entirely different profiling technique. This method explores the possibility of using very narrow resonances in proton-induced nuclear reaction cross section curves at intermediate ion energies. The principles are described in Fig. 6. The cross section curve of the $^{18}O(p,\alpha)^{15}N$ nuclear reaction curve displays several resonances, among them we select the most convenient one for profiling with nanometric resolution, namely the very narrow ($\Gamma \approx 100$ eV) resonance at 151 keV. This resonance can act as a natural energy filter, analogous to the artificial electrostatic analyzer.

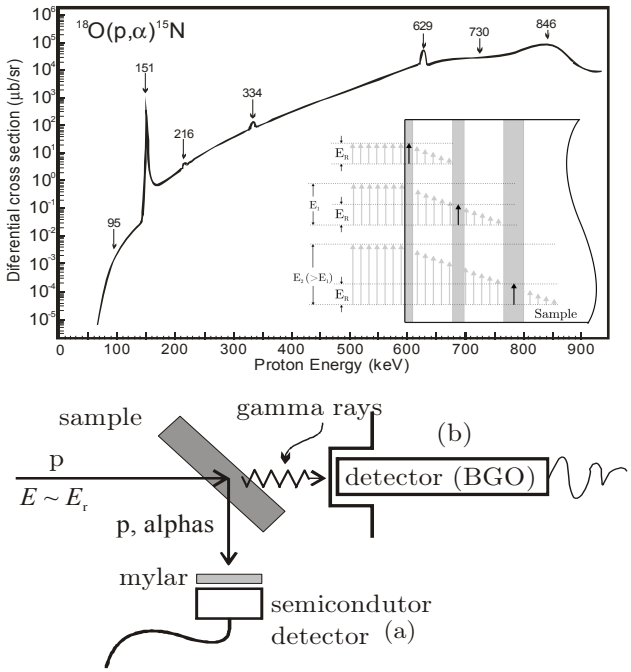

FIGURE 6. (top) cross section curve of the $^{18}O(p,\alpha)^{15}N$ nuclear reaction and sketch of the principle of NRP, (bottom) typical experimental arrangement for NRP.

If protons at the energy of the resonance reach the surface of a solid containing a certain distribution in depth of ^{18}O atoms, the nuclear reaction yield will be mainly due to reactions with ^{18}O atoms present in a narrow layer under the sample surface, whose thickness is proportional to the resonance width, on dE/dx, and on the energy stability of the proton beam. Raising the proton energy above the resonance energy, the ions will have to loose energy as they penetrate in the solid matter until reaching the resonance energy at a certain depth. The nuclear reaction yield will come now from the concentration of ^{18}O atoms in a layer situated at the depth where the ions reached the resonance energy. This new layer holds a width larger than the previous one due to straggling of the proton beam energy. Thus, by scanning the proton energy around the resonance energy, one can measure the excitation curve of the $^{18}O(p,\alpha)^{15}N$ nuclear reaction in this energy interval, which can be converted, with the proper energy loss law, in concentration of ^{18}O atoms in progressively deeper (and, unfortunately, broader) layers in the solid.

In the particular example used here, one can estimate the width of the first layer at the surface, or in other words the depth resolution therein, as approximately 0.7 nm. One of the reasons for a poorer energy resolution as compared to MEIS is the fact that only the energy lost by protons in the trajectory from the surface to the site of the nuclear resonant reaction event is taken into account. The energy loss of the outgoing reaction products is not measured, only the number of particles is counted. Therefore, the energy loss in NRP is typically half of the energy loss in an equivalent MEIS experiment, which degrades the accuracy for the determination of the former. A typical experimental setup is shown in Fig. 6 (bottom), including the possibility of measuring also gamma rays, since most of the used resonances are of the (p,γ) type.

Stochastic theory of ion energy loss, similar to that used for MEIS, gives:

$$N(E_0) = C(x)\sigma_0(E) * h(E_0) * \sum_0^\infty K_n f^{*n}(E - E_0)$$

where E is the proton energy and E_0 the energy of the resonance.

As an example we show in Fig. 7 the excitation curves of the $^{18}O(p,\alpha)^{15}N$ reaction around the resonance at 151 keV, for Al_2O_3, HfO_2, $HfAl_2O_5$, and $Hf_6Al_2O_{15}$ films on Si substrates on which 1.1 nm SiO_2 film was thermally grown previous to deposition. ^{18}O profiles C(x) used to simulate the different excitation curves with the above stochastic energy loss law are shown in the insets.

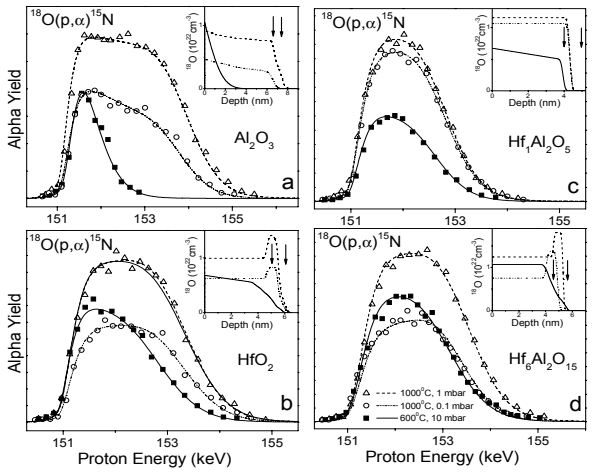

FIGURE 7. Excitation curves of the $^{18}O(p,\alpha)^{15}N$ nuclear reaction around the resonance at 151 keV, for Al_2O_3, HfO_2, $HfAl_2O_5$, and $Hf_6Al_2O_{15}$ films on 1.1 nm SiO_2 on Si. Profiles in the insets.

Another important example is high resolution profiling of Al in ultrathin Al_2O_3 films on Si, a challenging task that can be hardly tried with MEIS

due to the similar masses of both elements. The used resonance is the very narrow (Γ = 40 eV) resonance in the cross section curve of the $^{27}Al(p,\gamma)^{28}Si$ nuclear reaction at 404.9 keV, as shown in Fig. 8.

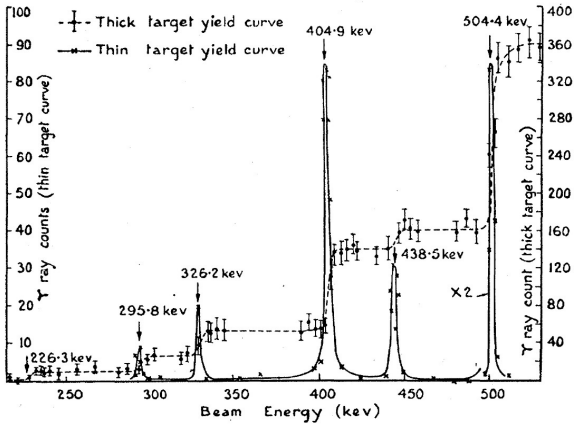

Figure 8. Cross section curve of the $^{27}Al(p,\gamma)^{28}Si$ nuclear reaction.

The excitation curves of the $^{27}Al(p,\gamma)^{28}Si$ nuclear reaction near the 404.9 keV resonance and the corresponding Al profiles are shown in Fig. 9 for progressively thicker Al_2O_3 films on Si. Depth resolution near the interface is 0.5 nm in this case. The corresponding MEIS spectra are also included in Fig. 9 for comparison, where one notices the overlap between Si and Al signals. It is noteworthy the absence of a background in the excitation curves of the $^{27}Al(p,\gamma)^{28}Si$ nuclear reaction.

High resolution profiling of O, Al, and Si ($^{29}Si(p,\gamma)^{30}P$ at 414 Kev, Γ = 100 eV) in Al_2O_3 films on Si, rapid thermal annealed in $^{18}O_2$ are shown in Fig. 10.

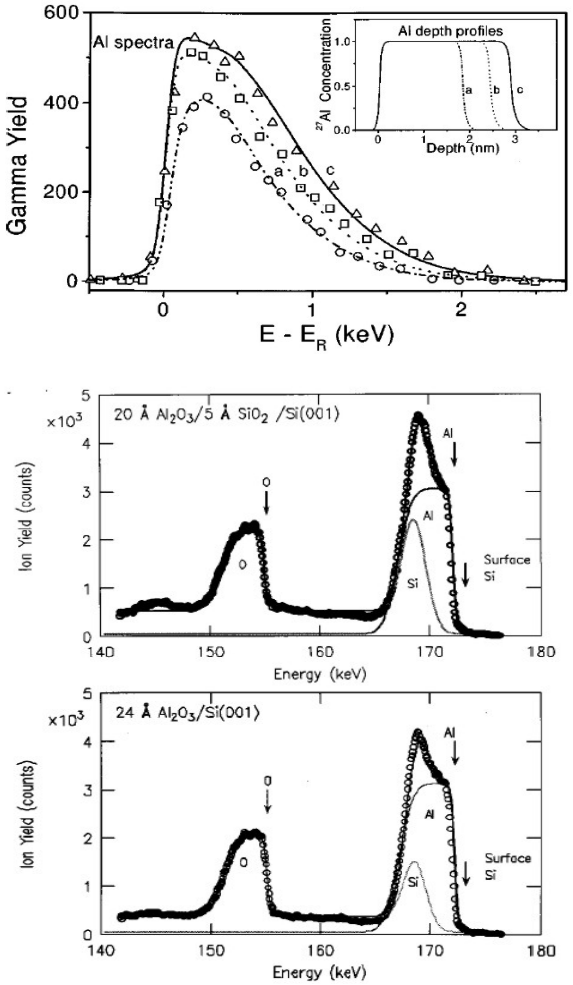

FIGURE 9. Excitation curves of the $^{27}Al(p,\gamma)^{28}Si$ nuclear reaction near the resonance at 404.9 keV (top) and corresponding MEIS spectra (bottom) obtained from Al_2O_3 films of different thicknesses deposited on Si. The corresponding Al depth profiles as determined by NRP are shown in the inset.

It is important to recall at this point the difference between MEIS and NRP profiling. In MEIS, all the chemical elements in the sample can be profiled with the same energy of the incident protons, constituting sometimes a great advantage and sometimes an undesired effect, like in ultrathin Al_2O_3, HfAlO, and $LaAlO_3$ films on Si, where the Si and Al signal overlap. On the other hand, in NRP the nuclear resonant reaction is selective of one particular light nuclide, while entirely insensitive to the others. On its turn, this is sometimes a great advantage, like in Al_2O_3, HfAlO, and $LaAlO_3$ films on Si, and sometimes a time consuming disadvantage. Moreover, subnanometric resolution profiling of heavy elements

is also impossible to reach with NRP, owing to the unacceptable low dE/dx at the high energies necessary to induce nuclear resonant reactions in these elements.

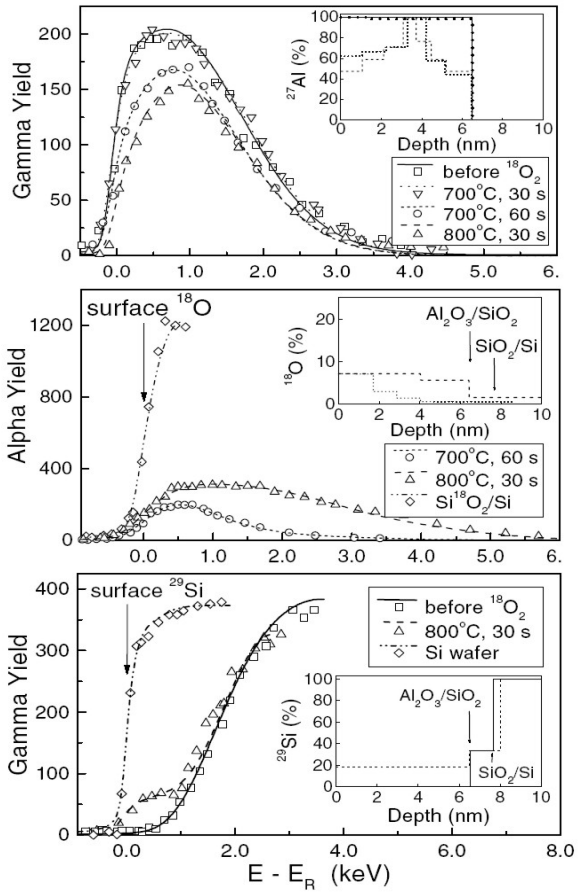

FIGURE 10. Excitation curves of the $^{27}Al(p,\gamma)^{28}Si$, $^{18}O(p,\alpha)^{15}N$, and $^{29}Si(p,\gamma)^{30}P$ nuclear reactions and the matching elemental depth profiles corresponding Al_2O_3/Si structures rapid thermal annealed in $^{18}O_2$.

Finally, high resolution profiling of N ($^{15}N(p,\alpha\gamma)^{12}C$ at 429 Kev, Γ = 120 eV) is illustrated in Fig. 11, for HfSiON films on a ultrathin layer of HfSiO^{15}N/Si annealed in different conditions.

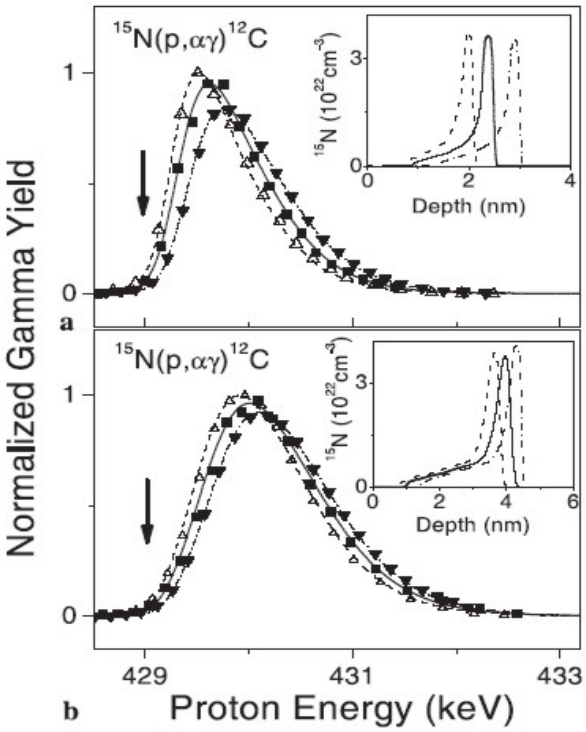

FIGURE 11. As-deposited samples (open triangles, dashed lines), annealed in N_2 at 600°C followed by rapid thermal annealed in O_2 at 1000°C (solid squares, solid lines), and rapid thermal annealed at 1000°C only (solid triangles, dash-dot lines). The arrows indicate the energy position corresponding to ^{15}N at the surface.

DISCUSSION AND CONCLUSIONS

The need for nano or subnanometric resolution profiling would increase in the forthcoming years, owing to the needs in ULSI research and development. Moreover, new areas like nanoelectronics and nanotechnology as a whole will also need to profile with high depth resolution. We presented in this article the principles and potentialities of two different techniques, both based on ion energy loss in matter, namely medium energy ion scattering (MEIS) and narrow resonant nuclear reaction profiling (NRP) which explore the so-called medium energy range of ion beams, where the ion energy losses have their maxima. The combined use of MEIS and NRP provide a rather complete tool to profile elements in ultrathin films or distributed in near surface regions with high depth resolution. Many other developments in these techniques are expected in near future as well as new methods, like for instance step by step chemical dissolution accompanied by determination of the total

amount of the species. This last technique is capable of providing even better depth resolution and therefore it should be investigated deeper.

The possibility of profiling elements with nano or subnanometric resolution is giving a significant contribution to solve many problems of research and development in MOS structures for advanced ULSI technology, which at present reach the nanometric scale.

REFERENCES

[1] W.-K. Chu, J. W. Mayer, and M.-A. Nicolet, Backscattering Spectrometry (Academic Press,New York, 1978).

[2] E. P. Gusev, H. C. Lu, T. Gustafsson, and E. Garfunkel, Physical Review B 52, 1759 (1994).

[3] Y. Kido and T. Koshikawq, Journal of Applied Physics 67, 187 (1990).

[4] G. Amsel, Nuclear Instruments and Methods in Physics Research 194, 1 (1982).

[5] J. F. van der Veen, Surface Science Reports 5, 199 (1985).

[6] R. P. Pezzi, M. Copel, and I. J. R. Baumvol, Submitted to Phys. Rev. B (2005).

[7] B. W. Busch, W. H. Schulte, T. Gustafsson, and C. Uebing, Nuclear Instruments and Methods in Physics Research 183, 88 (2001).

[8] B. W. Busch and T. Gustafsson, Surface Science 407, 7 (1998).

[9] M. Copel, M. Gribelyuk, and E. Gusev, Applied Physics Letters 76, 436 (2000).

[10] E. Gusev, M. Copel, E. Cartier, I. J. R. Baumvol, C. Krug, and M. Gribelyuk, Applied Physics Letters 76, 176 (2000).

[11] M. Copel, P. R. Varekamp, D. W. Kisker, F. R. McFeely, and M. M. Litz, K. E. Banaszak Holl, Applied Physics Letters 74, 1830 (1999).

[12] T. Gustafsson, H. C. Lu, B. W. Busch, W. H. Schulte, and E. Garfunkel, Nuclear Instruments and Methods in Physics Research 183, 146 (2001).

[13] J.-P. Maria, D. Wicaksna, A.I. Kingon, B. Busch, H. Schulte, E. Garfunkel, and T. Gustafsson, J. Appl. Phys 90, 3476 (2001).

[14] G. Amsel, G. Basttistig, and A. L'Hoir, Nuclear Instruments and Methods in Physics Research B 201, 325 (2003).

[15] H. H. Andersen, F. Besenbacher, P. Loftager, and W. M¨oller, Phys. Rev. A 21, 1891 (1980).

[16] B. Maurel, G. Amsel, and J. P. Nadai, Nuclear Instruments and Methods in Physics Research 197, 1 (1982).

[17] I. J. R. Baumvol, Surface Science Reports 36, 1 (1999).

[18] R. M. C. de Almeida and I. J. R. Baumvol, Surface Science Reports 49, 1 (2003).

[19] I. Vickridge and G. Amsel, Nuclear Instruments and Methods in Physics Research 45, 6 (1990).

[20] L. Miotti, K. P. Bastos, G. V. Soares, C. Driemeier, R. P. Pezzi, J. Morais, I. J. R. Baumvol, A. L. P. Rotondaro, M. R. Visokay, J. J. Chambers, et al., Applied Physics Letters 82, 4460 (2004).

[21] P. L. Grande, A. Hentz, G. Schiwietz, W. H. Schulte, B. W. Busch, D. Starodub, and T. Gustafsson, Phys. Rev. B 69, 104112 (2004).

[22] J. B. Marion and F. C. Young, Nuclear Reaction Analysis - Graphs and Tables (North-Holland, Amsterdam, 1968).

[23] B. Maurel, Ph.D. thesis, Universit´e Paris 7, Paris (1980).

[24] T. Nagao, J. T. Sadowski, M. Saito, S. Yaginuma, Y. Fujikawa, T. Kogure, T. Ohno, Y. Hasegawa, S. Hasegawa, and T. Sakurai, Phys. Rev. Lett. 93, 105501 (2004).